Parsing the Effects of Binding, Signaling, and Trafficking on the Mitogenic Potencies of Granulocyte Colony-Stimulating Factor Analogues

Casim A. Sarkar,[†,‡,#] Ky Lowenhaupt,[§] Peggy J. Wang,[†,‡] Thomas Horan,[⊥] and Douglas A. Lauffenburger*[,†,‡,§,∥]

Department of Chemical Engineering, Biotechnology Process Engineering Center, Department of Biology, and Biological Engineering Division, Massachusetts Institute of Technology, Cambridge, Massachusetts 02139-4307, and Department of Process Science, Amgen Inc., Amgen Center, Thousand Oaks, California 91320-1789

The pharmacodynamic potency of a therapeutic cytokine interacting with a cell-surface receptor can be attributed primarily to three central properties: [1] cytokine/receptor binding affinity, [2] cytokine/receptor endocytic trafficking dynamics, and [3] cytokine/receptor signaling. Thus, engineering novel or second-generation cytokines requires an understanding of the contribution of each of these to the overall cell response. We describe here an efficient method toward this goal in demonstrated application to the clinically important cytokine granulocyte colony-stimulating factor (GCSF) with a chemical analogue and a number of genetic mutants. Using a combination of simple receptor-binding and dose-response proliferation assays we construct an appropriately scaled plot of relative mitogenic potency versus ligand concentration normalized by binding affinity. Analysis of binding and proliferation data in this manner conveniently indicates which of the cytokine properties—binding, trafficking, and/or signaling—are contributing substantially to altered potency effects. For the GCSF analogues studied here, two point mutations as well as a poly(ethylene glycol) chemical conjugate were found to have increased potencies despite comparable or slightly lower affinities, and trafficking was predicted to be the responsible mechanism. A third point mutant exhibiting comparable binding affinity but reduced potency was predicted to have largely unchanged trafficking properties. Surprisingly, another mutant possessing an order-of-magnitude weaker binding affinity displayed enhanced potency, and increased ligand half-life was predicted to be responsible for this net beneficial effect. Each of these predictions was successfully demonstrated by subsequent measurements of depletion of these five analogues from cell culture medium. Thus, for the GCSF system we find that ligand trafficking dynamics can play a major role in regulating mitogenic potency. Our results demonstrate that cytokine analogues can exhibit pharmacodynamic behaviors across a diverse spectrum of "binding-potency space" and that our analysis through normalization can efficiently elucidate hypotheses for the underlying mechanisms for further dedicated testing. We have also extended the Black-Leff model of pharmacological agonism to include trafficking effects along with binding and signaling, and this model provides a framework for parsing the effects of these factors on pharmacodynamic potency.

Introduction

Therapeutic cytokines are capable of eliciting favorable cell responses such as proliferation, differentiation, or migration through specific, high-affinity interactions with cell-surface receptors. However, cytokine/receptor binding is only an initial step in the sequence of events ultimately leading to the cell response, as it is subsequently carried out via intracellular signaling cascades and often with attenuation due to endocytosis of the signaling complexes accompanied to some degree by subsequent lysosomal degradation of these molecules. This endocytic trafficking can deplete the extracellular ligand concentration over time and desensitize the cell to further stimulation by downregulating the number of cell-surface receptors. Therefore, the pharmacodynamic cell response does not necessarily correlate with binding affinity alone but can also be strongly influenced by associated mechanisms governing signal transduction and cytokine/receptor trafficking (*1*).

One cytokine of particular current importance is granulocyte colony-stimulating factor (GCSF), which stimulates elevation of neutrophil counts in patients presenting congenital neutropenia or in cancer patients

* To whom correspondence should be addressed. Tel: 617-252-1629. Fax: 617-258-0204. E-mail: lauffen@mit.edu.
[†] Department of Chemical Engineering.
[‡] Biotechnology Process Engineering Center.
[§] Department of Biology.
[∥] Biological Engineering Division.
[⊥] Department of Process Science.
[#] Present address: Biochemisches Institut, Universität Zürich, Winterthurerstrasse 190, CH-8057 Zürich, Switzerland.

10.1021/bp020017g CCC: $25.00
Published on Web 04/01/2003

undergoing chemotherapy (*2*). GCSF is a 19-kD member of the Group I cytokine superfamily, which is characterized by an antiparallel 4-α-helical bundle structure and includes other therapeutically important proteins such as erythropoietin and growth hormone (*3*). The target tissue for GCSF is bone marrow, where it binds with high affinity to the GCSF receptor (GCSFR) on neutrophilic precursor cells, inducing them to proliferate and differentiate into infection-fighting neutrophils (*4*). While this cytokine is an effective therapeutic agent, it suffers from an unusually short lifespan in vivo, due in large part to receptor-mediated endocytosis and degradation by circulating neutrophils that express GCSFR (*5, 6*). Thus, the efficacy of the drug is attenuated by this negative feedback mechanism, and consequently GCSF is commonly administered daily to maintain an adequate concentration in vivo (*6*). Many efforts in therapeutic drug design focus on maximizing the affinity of the drug for its intended target, but this may not necessarily be the optimal design criterion. In the case of re-engineering GCSF, this strategy may actually be counterproductive, as it may augment the receptor-mediated clearance of the drug by circulating neutrophils.

An alternative, or complementary, protein engineering approach that can directly affect the potency of a cytokine for local cell response (along with, in the particular case of GCSF, systemic pharmacokinetics by influencing receptor-mediated clearance) is the modification of ligand binding and/or trafficking in order to reduce receptor-mediated endocytosis and degradation. This modification could be an increased complex dissociation rate, a decreased complex internalization rate, or increased endosomal recycling of ligand molecules.

Two methods commonly utilized in modifying therapeutic proteins are the chemical conjugation of polymers such as poly(ethylene glycol) (PEG) (*7, 8*) and the substitution of amino acid residues in the protein. The attachment of PEG moieties to therapeutic proteins is expected to reduce renal clearance and mask proteolytic cleavage sites, thus enhancing pharmacokinetic properties in vivo (*9*). A GCSF analogue conjugated with PEG, termed SD/01, was found to be at least as efficacious as wild type and yet required significantly less frequent dosing (*9*, *10*).

Previous findings with epidermal growth factor, interleukin-2, and GCSF (*11*−*14*) suggest that, although amino acid substitutions can predictably modulate the binding affinity of a ligand for its receptor, an increased, decreased, or unchanged affinity does not necessarily directly correlate to superagonism, partial agonism, or full agonism, respectively (*1*). As noted in these examples, even mutations that result in no observable difference in receptor binding affinity can still modulate endocytic trafficking in a manner different from that of wild type, which in turn can alter pharmacodynamic response (*12*−*14*).

Our interest here is in analyzing the contributions of receptor-mediated properties (binding, signaling, and trafficking) of ligand analogues on pharmacodynamic cell response for the case of GCSF with the SD/01 chemical analogue along with amino acid mutants that sample a diverse range of pharmacodynamic behaviors, as measured by dose-response cell proliferation assays. In conjunction with receptor-binding experiments, we use this proliferation data to generate an affinity-normalized dose-response plot (ANDR plot). This methodology conveniently extracts the effects of binding affinity on potency, allowing inferences to be made about the relative contributions of signaling and trafficking. Not only is the inadequacy of binding affinity as a reliable predictor of potency clear from this methodology, but this scaled plot can be further employed to generate testable hypotheses concerning which cell-level properties are significantly modulating the potency of each analogue. For the GCSF analogues analyzed here, the ANDR analysis generates specific predictions regarding the trafficking properties for these ligands, and subsequent ligand depletion experiments for these mutants confirmed these guided inferences. In particular, we surprisingly find that SD/01 has a better pharmacodynamic response than wild type, despite a 3-fold lower receptor binding affinity. The ANDR plot predicts that this enhanced response is due to improved trafficking properties, and ligand depletion experiments reveal that SD/01 indeed has a lower degradation rate per cell than wild type, resulting in a significantly longer half-life. Thus, the PEG moiety on SD/01 not only improves the drug pharmacokinetics in vivo (*9*) but also appears to enhance its pharmacodynamic response through longer ligand half-life locally at the cell level. Additionally, using the ANDR analysis, we identify three mutants with even greater pharmacodynamic responses than SD/01 and successfully predict that reduced receptor-mediated depletion is likewise responsible for the improved potency of each.

Thus, the ANDR plot may serve as a generally useful diagnostic tool for deconvoluting the binding, signaling, and trafficking processes and for indicating which of these processes are significantly contributing to altered ligand potency. We mathematically extend the concept of the ANDR plot to generate a modified operational model of pharmacological agonism that details the effects of binding, signaling, and trafficking on cell response.

Materials and Methods

Preparation of GCSF Analogues. Both mutant and wild-type GCSF were refolded from inclusion bodies and purified as previously described (*15*). Additionally, to remove any trace of GCSF dimer, all samples were subjected to gel filtration on a 35/600 Superdex 75 column (Pharmacia) run in 25 mM sodium acetate, 100 mM sodium chloride, pH 5.0. SD/01 was prepared as described (*16*). The entire extracellular domain of the GCSF receptor was expressed in Chinese hamster ovary cells and purified from conditioned media as previously reported (*17*).

Cell Line and Culture. The GCSF-dependent suspension cell line OCI/AML1 was used for all experiments. Minimum essential medium alpha (MEMα), L-glutamine, penicillin-streptomycin, fetal bovine serum (FBS), and phosphate-buffered saline were obtained from Life Technologies, Inc. Isotonic solution for the Coulter counter (ISOTON II, Coulter Diagnostics, Hialeah, FL) was obtained from Curtin Matheson Scientific Inc. (Houston, TX). Every 3−4 days, cells were diluted to 10^5/mL in MEMα supplemented with 20% FBS, 200 mM L-glutamine, 100 units/mL penicillin, 100 μg/mL streptomycin, and 270 pM GCSF and incubated in a humidified atmosphere with 5% CO_2 at 37 °C.

Binding Experiments. The interaction between GCSF and GCSFR was studied using the BIAcore 2000 (BIAcore, Uppsala, Sweden). Wild-type GCSF, modified to include a $(His)_6$-tag, was coupled to the BIAcore NTA chip in the presence of nickel. Binding of GCSFR to coupled GCSF was measured directly in eluent buffer (10 mM HEPES, 0.15 M NaCl, 50 μM EDTA, 0.005% Surfactant P-20 (BIAcore, Uppsala, Sweden), pH 7.4). Varying concentrations of GCSFR were passed over a surface with

300 RU of GCSF attached. It was not possible to dissociate the GCSFR from the GCSF without denaturing both components; therefore, the surface was stripped with 0.35 M EDTA and fresh $(His)_6$-GCSF was bound between each concentration of receptor. Binding was measured at a flow rate of 20 μL/min for 5 min, followed by a 50 min dissociation phase. The K_D values were calculated from the binding curves, which were analyzed by BIAeval version 3.0 (BIAcore, Uppsala, Sweden) using a Langmuir binding model with sloping baseline. All experiments were performed in triplicate.

The equilibrium binding constant for each analogue was obtained by solution affinity measurements. Under conditions where binding is limited by mass transport, the rate of binding is proportional to the concentration of analyte. The rate of binding for various concentrations of GCSFR was determined in NTA buffer at a flow rate of 5 μL/min, with 1000 RU of $(His)_6$-GCSF attached to the surface. A fresh surface was prepared for each data point. A standard curve of receptor concentration versus binding was used to determine the concentration of free GCSFR; the K_D for each analogue was then calculated from a plot of free receptor versus initial ligand concentration by fitting the data to an equation describing equilibrium mixtures of GCSFR and ligand: $R_{free} = ((R_0 - L_0 - K_D) + \sqrt{(R_0-L_0-K_D)^2+4R_0K_D})/2$, where R_0 and L_0 are the initial concentrations of receptor and ligand, respectively. Mixtures of GCSF or an analogue with 2 nM GCSFR were equilibrated at room temperature for at least 30 min and tested as described for GCSFR. Comparison of samples equilibrated for 30 min or up to 24 h showed no systematic variation. All samples were analyzed three times, and all experiments were carried out in triplicate. K_D values were determined using BIAeval version 3.0, and all were best fit by a 1:1 binding model.

Cell Proliferation Experiments. Cells were passaged into supplemented MEMα medium without GCSF 24 h prior to the initiation of the cell proliferation experiments, at which point parallel plates of cells at a density of 10^5/mL were incubated in supplemented MEMα medium with a known concentration of wild-type GCSF or analogue (L_0 = 1000, 500, 250, 125 pM). For each experiment, duplicate plates were prepared for each sample, and the plates were stored in a humidified atmosphere with 5% CO_2 at 37 °C. After 3 days, one plate of each sample was diluted 1:15 in Isoton II and counted using a Coulter counter to determine cell density. This procedure was repeated for the second set of samples after 7 days. The error bars for all plots represent the standard deviations from at least two independent experiments.

Ligand Depletion Experiments. Cells were passaged into supplemented MEMα medium without GCSF 24 h prior to the initiation of the ligand depletion experiments, at which point parallel flasks of cells at a density of 10^5/mL were incubated in supplemented MEMα medium with 270 pM wild-type GCSF or analogue. After 3 and 6 h, an aliquot of each medium supernatant, obtained after centrifugation to pellet cellular debris, was stored at −20 °C for later analysis. After each 24-h period from the start of each experiment, the cell density in each flask was monitored using a Coulter counter and an aliquot of each medium supernatant was stored at −20 °C for later analysis. This was repeated every 24 h for 6 days. The concentration in each medium supernatant sample was quantitated using enzyme-linked immunosorbent assay (ELISA) kits obtained from R&D Systems (Minneapolis, MN). Using these data, the macroscopic ligand degradation rate constant per cell (k_{deg}) was determined using the equation $dL/dt = -k_{deg} \cdot \rho(t)$, where L is the ligand concentration in the medium and $\rho(t)$ is the time-variant cell density. Wild-type GCSF depletion experiments performed using the YT-2C2 suspension cell line, which is GCSF-independent and does not express GCSFR, revealed greater than 80% intact ligand after 6 days (data not shown); therefore, ligand depletion from the medium indeed appears to be driven by receptor-mediated trafficking and not by differences in extracellular ligand stability.

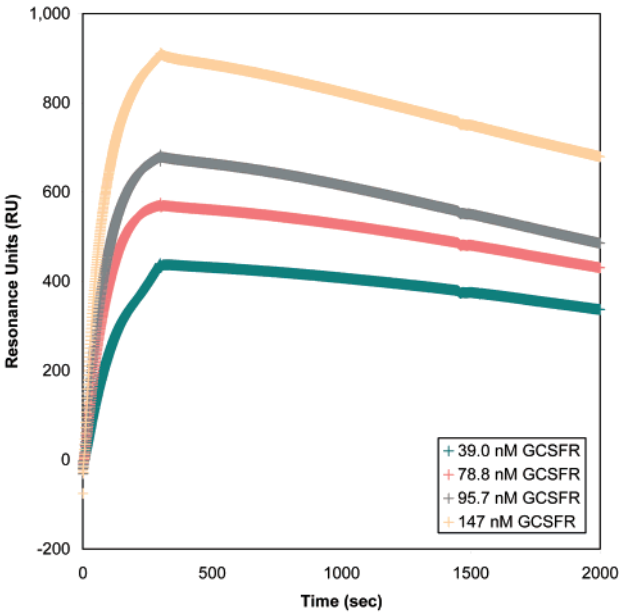

Figure 1. Surface plasmon resonance data for determining the effective K_D of wild-type GCSF. Real time measurements of binding of GCSFR to $(His)_6$-GCSF were performed as described. 39.0 nM (teal), 78.8 nM (rose), 95.7 nM (gray) and 147 nM (beige) GCSFR flowed over a surface modified with $(His)_6$-GCSF. These representative data show a K_D of 130 pM.

Results

Equilibrium Binding Affinities for Wild Type and Analogues. The equilibrium dissociation constants (K_D = inverse equilibrium affinity constant) for SD/01 and several GCSF point mutants (E20A, G27A, E34A, E47A, and L51E) were determined by surface plasmon resonance measurements (data for wild type shown in Figure 1). The K_D values for the analogues, normalized to wild type, are given in order of increasing binding affinity from left to right in Figure 2. Interestingly, SD/01 was found to have a 3-fold lower affinity than wild type. Thus, it appears that the PEG moiety reduces the receptor binding affinity of SD/01, but this does not appear to impact its clinical efficacy (*9*). The K_D values for the mutant analogues range from greater than 360-fold lower affinity than wild type to comparable affinity. If increased binding affinity correlated positively with increased potency, we would expect to see, in a cell proliferation assay using each mutant in Figure 2, a monotonic increase in cell density going from E20A to G27A.

Cell Proliferation in Response to Wild Type and Analogues. To determine how modulation of the receptor binding affinity affects mitogenicity in culture, we tested wild-type GCSF and the analogues in a dose-response cell proliferation assay with the GCSF-dependent cell line OCI/AML1. Using initial ligand concentrations of 1000,

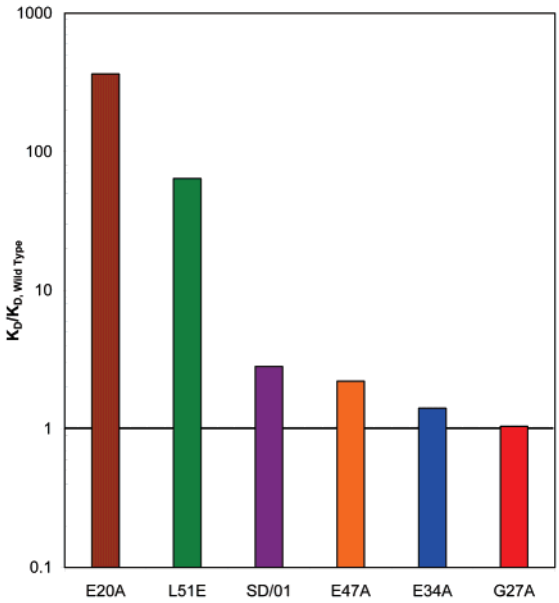

Figure 2. Effective K_D data for all GCSF analogues, normalized to wild type. Analogues are arranged in order of increasing binding affinity from left to right. Color coding: E20A (brown), L51E (green), SD/01 (purple), E47A (orange), E34A (blue), and G27A (red).

500, 250, and 125 pM with no replenishment, we incubated cells at an initial density of 10^5/mL. The resulting cell densities for wild type after 3 and 7 days are given in Figure 3A. The cell densities for the analogues, normalized to corresponding wild-type values at the same initial ligand concentration, are given in Figure 3B ($t = 3$ days) and 3C ($t = 7$ days). The order of the mutants is the same as in Figure 2 (increasing binding affinity from left to right); however, it is especially clear from Figure 3C that mitogenicity does not positively correlate with binding affinity.

Most surprisingly, L51E binds with much lower affinity than wild type (Figure 2) but elicits a pharmacodynamic response essentially equal to wild type at 3 days (Figure 3B) and greater than wild type at 7 days (Figure 3C). Conversely, E47A binds with similar affinity to wild type (and with much higher affinity than L51E) yet is less potent than expected at both timepoints (Figure 3B and 3C). An initial dose of 125 pM E34A, which has a receptor binding affinity similar to wild type, elicits a cellular response 2-fold greater than that achieved with the same dose of wild type after 7 days (Figure 3C).

No difference in cell density was observed between wild type and SD/01 after 3 days at any of the concentrations. In fact, if we extend the timepoint to 7 days, we find that the cell density for each sample treated with SD/01 was greater than that treated with an equivalent concentration of wild type (Figure 3C). This demonstrates that a 3-fold reduction in binding affinity does not affect the overall mitogenic potency of SD/01.

These counterintuitive results suggest that other processes, namely, trafficking and signaling, are significantly affecting the pharmacodynamic potency, since the results of these dose-response proliferation assays cannot be explained by binding affinity alone. Using both the binding affinity and proliferation results, we generated a scaled plot to help assess the contributions of these other processes to the overall pharmacodynamic response.

Generation of the Affinity-Normalized Dose-Response (ANDR) Plot. For each analogue, the cell proliferation experiments were performed with the same initial ligand concentrations (L_0 = 1000, 500, 250, 125 pM). However, these values are not the best indicators of the concentrations "seen" by the cells; a cell senses the ligand concentration through the number of complexes formed with its surface receptors. Since the analogues have a range of K_D values, a better estimate of the ligand concentration is the nondimensionalized L_0/K_D. Thus, although the same initial ligand concentrations were used for each analogue (an 8-fold span between 125 and 1000 pM), the value for L_0/K_D ranges from 0.002 to 12 (a 6000-fold span). The plot of cell density versus the logarithmically scaled nondimensional ligand concentration (L_0/K_D) after 3 days is given in Figure 4A and that after 7 days is given in Figure 4B, with the shaded regions highlighting ligands with *effective* ligand concentrations in the same range as wild type. In Figure 4B, the E20A mutant, which binds over 360-fold more weakly than wild type, is predictably less potent, lying in the bottom left corner of the plot. The L51E mutant, which binds over 60-fold more weakly than wild type, is nonetheless more potent. In the shaded region of Figure 4B, we find that the G27A and E34A mutants, as well as the SD/01 analogue, are more potent than wild type, while E47A is less potent. For these particular ligands at 7 days, we can generate the ANDR plot by further scaling the mitogenic response on the y-axis.

The appropriate y-coordinate scaling of each data point should be the corresponding wild-type cell density at the same *effective* ligand concentration. Because the K_D values are different for the mutants, we do not have a direct comparison between wild type and the mutants, and we therefore interpolate the corresponding cell densities from the wild-type curve. Although a full dose-response curve on this plot would appear sigmoidal, we can reasonably assume that the four wild-type data points lie within the pseudolinear portion in the middle of the full curve. We therefore fit the wild-type data from Figure 4B to a linear equation correlating ρ_{WT} to $\log(L_0/K_D)$, with resulting $r^2 = 0.999$. For each data point in Figure 4B with an x-coordinate that lies in the wild-type range of L_0/K_D (i.e., those data points in the shaded region), the corresponding y-coordinate for each such data point was normalized to the ρ_{WT} value calculated from this equation using the x-coordinate value. This is the resulting ANDR plot and is shown in Figure 4C. The dashed lines and open circles represent extrapolations outside of the wild-type L_0/K_D range and therefore may not necessarily be quantitatively precise but are included to show all four points in each curve. This method of normalizing the y-axis should fully cancel out any contributions of binding affinity, and therefore the differences in the curves are attributable to either trafficking or signaling differences (or both).

At high effective ligand concentrations ($L_0/K_D \approx 10$), trafficking effects should be minimal as the ligand concentration is in great excess relative to the K_D and we expect receptor-mediated processes to become saturated. Consequently, we can infer that the differences in potency at high effective ligand concentrations are due to intrinsic signaling. Differences in potencies between G27A and E34A and wild type are small at this point, suggesting that the mutants are not significantly superior signal transducers upon receptor binding. Conversely, at an L_0/K_D value near 1, trafficking and depletion of the ligand can affect potency substantially, and at this concentration the mutants are twice as potent as wild type. Since we infer that the enhanced potency is not due to differences in binding affinity or signaling,

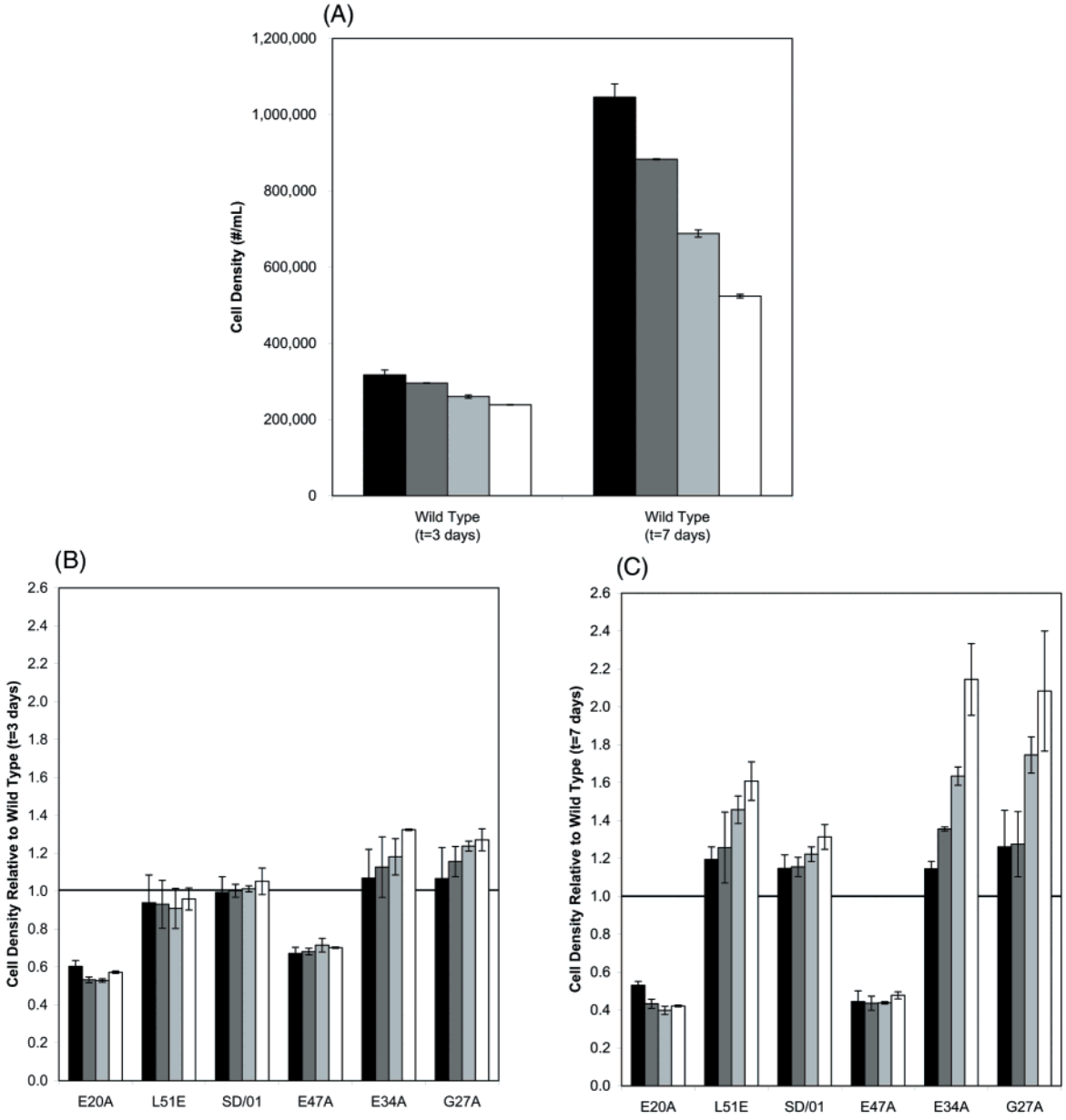

Figure 3. (A) Cell proliferation data for wild type ($t = 3$ and 7 days), (B) proliferation data for analogues normalized to wild type ($t = 3$ days), and (C) proliferation data for analogues normalized to wild type ($t = 7$ days). The initial cell density for all samples was 10^5/mL, and initial ligand concentrations used were 1000 pM (solid black), 500 pM (dark gray), 250 pM (light gray), and 125 pM (white).

we can assert that this superagonism is a consequence of improved trafficking, which would result in less depletion per cell and possibly a longer ligand half-life. Through this reasoning, we conjecture that mutants with such negative sloping curves have improved trafficking properties. Thus, we also expect to see a trafficking improvement for SD/01, although perhaps not as great of an enhancement. Conversely, the slope of the E47A mutant is almost zero, suggesting that its trafficking properties are comparable to those of wild type; otherwise, we would expect to see some difference in potency at higher L_0/K_D (where trafficking effects are masked) and at lower L_0/K_D (where trafficking effects are important). This analysis implicates a poorer signaling mechanism for the reduced potency of E47A.

The two mutants to the left of the shaded region in Figure 4B are more difficult to analyze, because we can no longer rule out differences in binding affinity in explaining altered potencies (these mutants share no common L_0/K_D value with wild type for comparison purposes). The E20A mutant in the bottom left quadrant is perhaps a predictable result, with such a large reduction in binding affinity leading to insufficient proliferative signals. The binding and proliferation results here are consistent with other findings that confirm that E20 is critical to receptor recognition and ligand function (*18*, *19*). While the L51E mutant is not included in the ANDR plot because it did not fall into the shaded area in Figure 4B, we nevertheless expect this more potent mutant to have a reduced depletion rate per cell because the large reduction in binding affinity should decrease the flux of ligand molecules into the cells.

Ligand Depletion Calculations for GCSF Mutants. To test trafficking predictions made through analysis of the ANDR plot, ligand depletion experiments using enzyme-linked immunosorbent assays were performed. The depletion profiles and the corresponding cell proliferation curves are shown in Figure 5A and 5B,

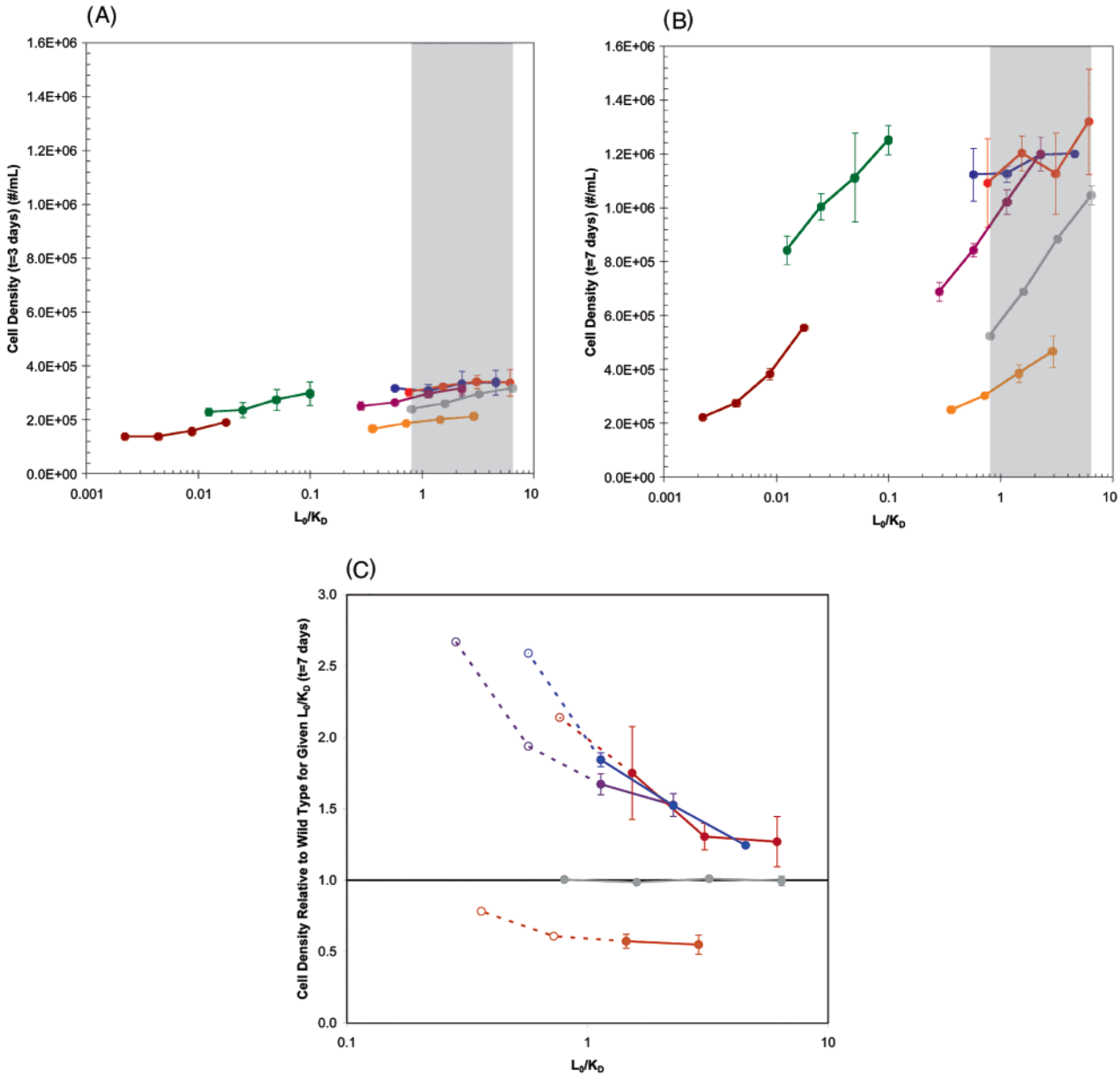

Figure 4. (A) Cell proliferation data (t = 3 days) plotted as a function of effective initial ligand concentration (L_0/K_D). (B) Cell proliferation data (t = 7 days) plotted as a function of effective initial ligand concentration (L_0/K_D). (C) ANDR plot for t = 7 days. The ANDR plot is generated by normalizing the pharmacodynamic response of the analogue by that of wild type at the same effective initial ligand concentration and plotting this versus the effective initial ligand concentration. Color coding: E20A (brown), L51E (green), SD/01 (purple), E47A (orange), E34A (blue), G27A (red), and wild type (gray).

respectively. These data were used to calculate the macroscopic ligand degradation rate constant per cell, k_{deg} (see Materials and Methods). Consistent with the predictions, the E47A mutant was found to have a degradation rate constant comparable to that of wild type. The hypothesis that the G27A and E34A mutants have improved trafficking properties is supported by the substantially smaller values of k_{deg} for each of these ligands. L51E is also shown to have a longer half-life per cell, but this is likely due to its significantly lower binding affinity since this parameter could not be effectively ruled out. The improvement in trafficking for SD/01 was predicted to be not as great, and this is highlighted by an intermediate value of k_{deg}. While SD/01 has been shown to have reduced nonspecific clearance (*9*), our findings suggest that receptor-mediated clearance of GCSF is also reduced by the addition of the PEG moiety. Furthermore, these results suggest that the PEG moiety would contribute not only to the improved systemic pharmacokinetic properties of the drug, as has been widely appreciated, but would also serve to enhance local target-cell pharmacokinetics and pharmacodynamics.

Discussion

Increased efficiency in evaluation of therapeutic protein analogues is desirable across a spectrum of required properties including pharmacokinetics, pharmacodynamics, and toxicity. For the case of GCSF, a highly important example clinically, a new chemical analogue (SD/01) has been demonstrated to exhibit enhanced effectiveness in vivo (*9*), with the enhancement attributed to improved pharmacokinetic behavior, specifically, longer half-life in the systemic circulation. It is not clear, however, what underlying cell-level mechanism is responsible for this longer half-life. Both the actual target cell-type for GCSF

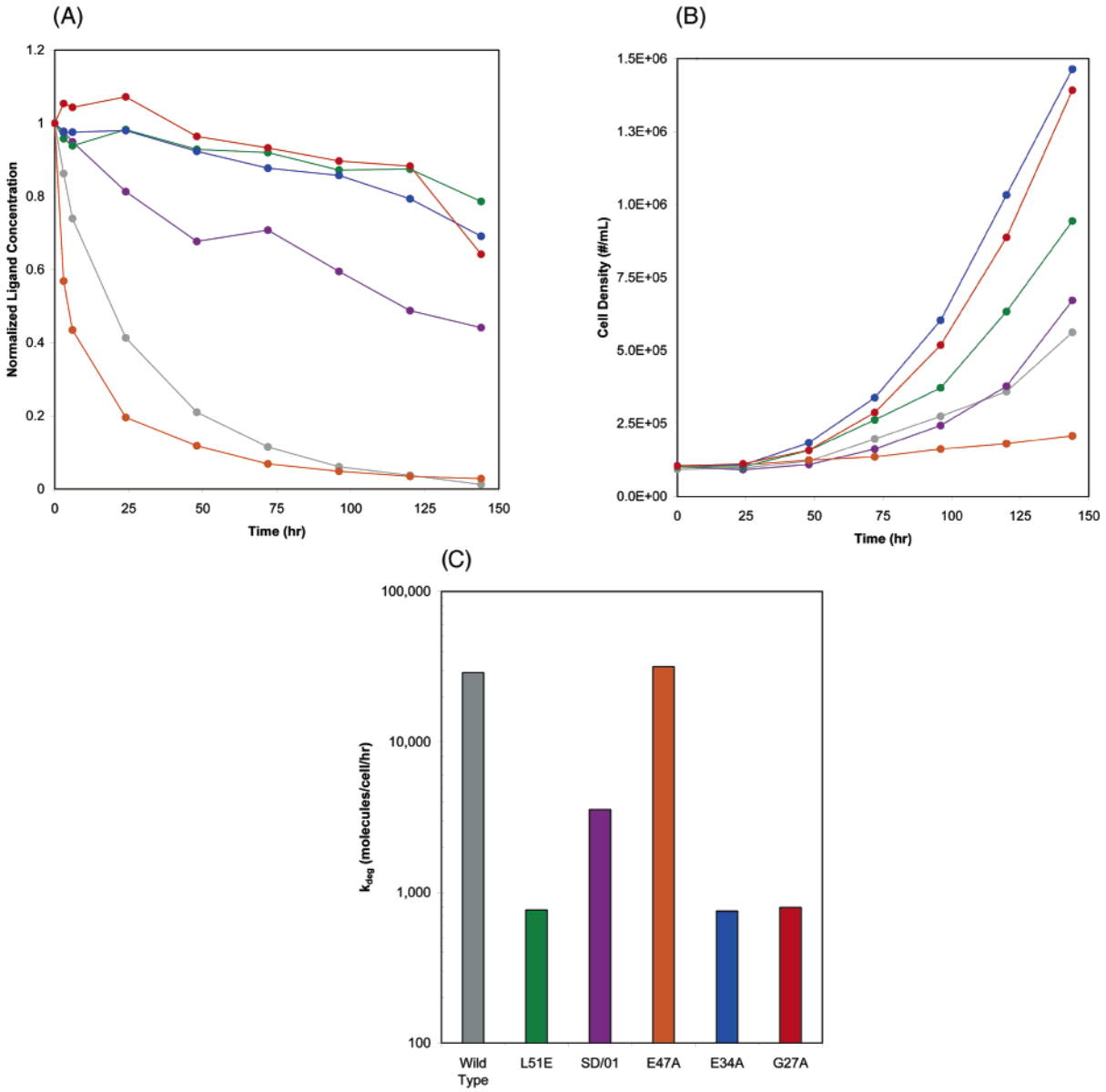

Figure 5. (A) Ligand depletion profiles for wild type and mutants. (B) Corresponding cell proliferation profiles for part A. (C) Calculated macroscopic ligand degradation rate constant per cell (see Materials and Methods). The initial ligand concentration was 270 pM for all samples, and the initial cell density was 10^5/mL. Color coding: L51E (green), SD/01 (purple), E47A (orange), E34A (blue), G27A (red), and wild type (gray).

action, neutrophilic precursor cells in the bone marrow, and the resulting mature neutrophils circulating in the bloodstream express surface GCSFR that can bind the ligand leading to its endocytic degradation (*5*, *6*). Thus, the enhanced effectiveness could be due to a combination of improvements in both pharmacodynamic and pharmacokinetic behaviors. We were accordingly motivated to quantitatively analyze pharmacodynamic properties of SD/01 along with analogues generated by amino acid substitution. As shown, SD/01 was found to have greater mitogenic potency than wild type (Figure 3C), and this is likely due to its reduced cell-mediated depletion (Figure 5). These findings suggest that the greater in vivo effectiveness of SD/01 may be due to improved pharmacodynamics, as well as the enhanced pharmacokinetics previously considered. Three point mutants of GCSF (G27A, E34A, and L51E) exhibit even greater potencies than SD/01 in culture, suggesting that they may be promising candidates for PEG-conjugation and in vivo testing. Moreover, these results present the possibility that analogues of GCSF, as well as other therapeutic cytokines, exhibiting superior pharmacodynamic properties might be engineered more generally, by appropriate influence of at least one of three central properties: (1) cytokine/receptor binding affinity, (2) cytokine/receptor endocytic trafficking dynamics, and (3) cytokine/receptor complex signaling. Since quantitative information connecting signaling metrics with cell responses is essentially unavailable at the present time and since increasing binding affinity may rarely be a productive avenue for providing greater cell response (*20*), guided manipulation of endocytic trafficking offers an exceptionally promising direction toward this objective (*14*).

As we have shown through analysis of the features of the curves in the ANDR plot, we can deconvolute the processes of binding, signaling, and trafficking and suggest which of these are contributing substantially to altered ligand potency. We were able to generate hypotheses from the plot and then successfully tested our predictions using ligand depletion experiments, which demonstrated either the presence (L51E, E34A, G27A,

and SD/01) or absence (E47A) of beneficial cellular trafficking effects.

The results presented here for GCSF are part of a more general model for agonist-induced cell responses, and we can gain some greater insight into the contributions of binding, signaling, and trafficking to pharmacodynamic response through a mathematical analysis. For a given cell, extracellular ligand (L) elicits a cellular response by first binding to free surface receptors to form complexes (C):

$$C = \frac{R_0 L}{K_D + L} \tag{1}$$

where the K_D is the inverse equilibrium affinity constant and R_0 represents the total number of surface receptors. Utilizing this equilibrium relationship between occupied receptors and free ligand, Black and Leff developed an operational model of pharmacodynamic response that transduces the signals from the complexes into a cell response (*21*). They showed that such a transducing model must retain a hyperbolic form in order to match experimental observations:

$$\frac{E}{E_{max}} = \frac{C}{K_E + C} \tag{2}$$

where E/E_{max} represents the normalized pharmacological effect and K_E is the number of occupied receptors required to generate a half-maximal response. The result of combining eqs 1 and 2 is

$$\frac{E}{E_{max}} = \frac{\left(\frac{\tau}{\tau+1}\right)\left(\frac{L}{K_D}\right)}{\frac{1}{\tau+1} + \frac{L}{K_D}} \tag{3}$$

where $\tau = R_0/K_E$ is referred to as the "transducer function". It should be noted that for many agonists such as cytokines the number of complexes necessary to generate a half-maximal response is typically a very small fraction of the total (*20*), and therefore τ is much greater than 1 for such ligands. Therefore, the Black-Leff model accounts for the contributions of binding (through K_D) and signaling (through τ) but not trafficking.

In Figure 6A, we illustrate dose-response curves for hypothetical analogues of an agonist, where the normalized pharmacological response is plotted against the effective ligand concentration. One of the features of eq 3 is that the maximum normalized response and the concentration for half-maximal response (EC_{50}) are not independent, as they are both governed by the parameter τ. However, if we examine ligands "*a*" and "*b*" in Figure 6A, we find that at high effective ligand concentrations both ligands elicit equal cell responses, but at intermediate concentrations ligand "*a*", with a greater than 7-fold lower EC_{50}/K_D, is much more potent than ligand "*b*". This example highlights the shortcomings of the Black-Leff model, in that it cannot be used to fit the dose-response curves for both of these hypothetical ligands.

We note that the derivation of the Black-Leff model, by using eq 1, neglects endocytic trafficking of surface complexes and free receptors, which can modulate the pharmacological response. Since full incorporation of the equations governing cellular trafficking of ligand and receptor molecules does not allow for an analytical solution, we derive an operational model (see Appendix) based on some simplifying assumptions that nonetheless

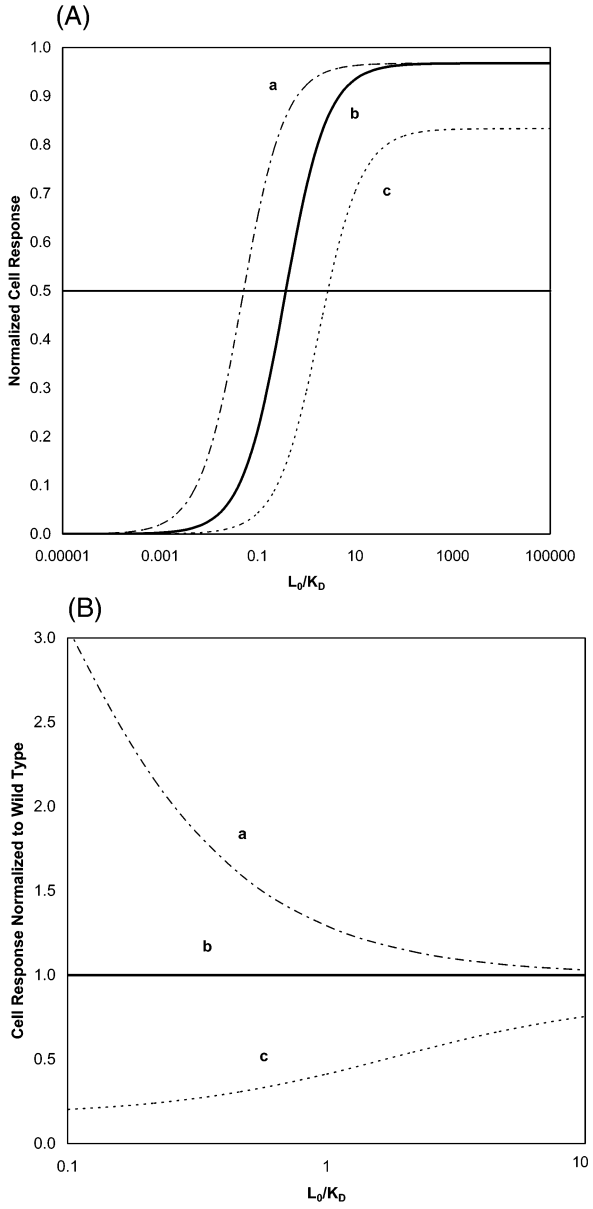

Figure 6. (A) Dose-response curves for hypothetical analogues of an agonist. Ligand "*a*" has $\tau = 30$ and $\kappa = 0.5$; ligand "*b*" has $\tau = 30$ and $\kappa = 10$; and ligand "*c*" has $\tau = 5$ and $\kappa = 10$. The parameters τ and κ are for the modified operational model (eq 5) in the Discussion. (B) The dose-response curves in part A are normalized to the curve for ligand "*b*".

can capture some of the impact of cellular trafficking on the pharmacological response. In the presence of constitutive receptor internalization, constant ligand concentration, constant cell density, and no endocytic recycling, the quasi-steady-state number of complexes will be

$$C_{ss} = \frac{R_0 L}{(\kappa + 1)K_D + L} \tag{4}$$

where κ is the ratio of the internalization rate constant to the complex dissociation rate constant. Substitution of this expression into eq 2 yields

$$\frac{E}{E_{max}} = \frac{\left(\frac{\tau}{\tau+1}\right)\left(\frac{L}{K_D}\right)}{\frac{\kappa+1}{\tau+1} + \frac{L}{K_D}} \tag{5}$$

A comparison of eqs 3 and 5 reveals that this modified operational model captures the contributions of binding and signaling in the same manner as the original model; however, the parameter κ introduces the dependence of the pharmacological response on cellular trafficking. In this particular derivation, κ represents the ratio of internalization to dissociation in the absence of endocytic sorting. However, more generally, it can be instructive to think of κ as an effective trafficking parameter that represents the ratio of net endocytosis (internalization minus recycling) to surface dissociation. Cell-mediated ligand depletion can be reduced by increasing complex dissociation, decreasing complex internalization, or increasing ligand recycling. All three of these modifications would decrease κ, suggesting that a fruitful approach to ligand design would be to reduce κ, and we have previously described a rational strategy for achieving this (*14*). Indeed, we can clearly see from eq 5 that the most potent agonist would have a maximum value of τ and a minimum value of κ.

Furthermore, using eq 5, we can uniquely describe two ligands with different maximum normalized responses but the same EC_{50} value or with the same maximum normalized response but different EC_{50} values (e.g., curves "*a*" and "*b*" in Figure 6A ($\tau = 30$ and $\kappa = 0.5$ for "*a*" and $\tau = 30$ and $\kappa = 10$ for "*b*")). Curve "*c*" in Figure 6A, with different maximum normalized response and different EC_{50} (corresponding to $\tau = 5$ and $\kappa = 10$) is also uniquely fit by the modified model.

If curve "*b*" in Figure 6A were the wild-type ligand, normalization of all three curves in Figure 6A to curve "*b*" would result in Figure 6B. We note that curves "*a*" and "*b*" have the same value for τ (same signaling properties), and curves "*b*" and "*c*" have the same value for κ (same trafficking properties). Although some of the assumptions in the model are not valid for the particular GCSF analogue results presented here, we nonetheless observe some qualitative agreement between Figures 4C and 6B. If a full set of equations for ligand/receptor trafficking were necessary, the pharmacological response, as predicted by the equations, could be solved numerically. However, the analytically derived operational model provides some insight into the three agonist properties that can impact the pharmacological response, and in this respect, κ represents the contribution of cellular trafficking. It is important to know whether binding, signaling, or trafficking properties are improved when assessing the therapeutic potential of ligand analogues in the laboratory, as the bottleneck in potency in vivo may not be spread across all three of these contributions. For clinical therapeutics such as GCSF that suffer substantially from cell-mediated depletion in vivo, their potencies can be enhanced by improving cellular trafficking properties and here we have found four analogues of GCSF to have reduced depletion per cell in comparison to wild type. More generally, the ANDR plot and the modified Black-Leff model of pharmacological agonism presented here should be useful diagnostic tools for screening ligands, not just by binding affinity and potency, which we have shown here not to correlate well, but also by inference of some signaling and trafficking properties.

Acknowledgment

The authors gratefully acknowledge David Brems, Daniel Kamei, and Dane Wittrup for helpful discussions and Ernest McCulloch for providing the OCI/AML1 cell line. This work was supported by a Fannie & John Hertz Foundation Fellowship to C.A.S. and a grant from the Amgen/MIT partnership to D.A.L.

Appendix

The governing mass-action kinetic equations for surface receptors (R), surface complexes (C), and extracellular ligand (L) in the absence of recycling and cell proliferation are

$$\frac{dR}{dt} = -k_f LR + k_r C - k_{eR} R + V_s \tag{A.1}$$

$$\frac{dC}{dt} = k_f LR - k_r C - k_{eC} C \tag{A.2}$$

$$\frac{N_A}{\rho}\frac{dL}{dt} = -k_f LR + k_r C \tag{A.3}$$

where k_f is the complex association rate constant, k_r is the complex dissociation rate constant, k_{eR} is the free receptor internalization rate constant, V_s is the receptor synthesis rate, k_{eC} is the complex internalization rate constant, N_A is Avogadro's number, and ρ is the cell density. To achieve an analytical result for the operational model, several assumptions were invoked for the cellular trafficking dynamics. First, L was assumed to be constant in this analysis ($dL/dt = 0$), as in the Black-Leff model. While trafficking effects will in many cases deplete the ligand over time, this is a conservative assumption as ligand depletion (and cell proliferation) will tend to accentuate differences predicted by the model, particularly at longer times. Furthermore, receptor internalization was assumed to be constitutive; in other words, the internalization rate constants for free receptor and occupied receptor were taken to be equal ($k_e = k_{eR} = k_{eC}$). While many agonists induce a higher internalization rate constant of occupied receptors, this would serve to downregulate the total number of surface receptors (R_T not constant over time) and consequently have a more dramatic effect not only on cellular trafficking but also on the parameter τ in the model. These assumptions allow us to approximate the impact of cellular trafficking on the operational model analytically.

We can show by summing eqs A.1 and A.2 that the total number of surface receptors at any given time is constant and is equal to the initial number of surface receptors ($R + C = R_T = R_0 = V_s/k_e$):

$$\frac{d(R + C)}{dt} = V_s - k_e(R + C) \tag{A.4}$$

However, at $t = 0$, $R + C = R_0 = V_s/k_e$. Therefore, $d(R + C)/dt$ is zero throughout the time course. Consequently, we can rewrite the differential equation for C as

$$\frac{dC}{dt} = k_f LR_0 - (k_f L + k_r + k_e)C \tag{A.5}$$

The solution to this equation is straightforward, but we note that the time constant in this equation is $1/(k_f L + k_r + k_e) < 1/k_r$. Since C will be essentially at equilibrium after three time constants, we find that the time to reach this state is at most $3/k_r \approx 30$ min for an average dissociation rate constant. Since this is much faster than the typically measured pharmacological response, we are

justified in using the quasi-steady-state number of complexes in our operational model:

$$C_{ss} = \frac{R_0 L}{\left(\frac{k_e}{k_r} + 1\right) K_D + L} \quad \text{(A.6)}$$

This is identical to eq 4 in the main text.

References and Notes

(1) Lauffenburger, D. A.; Fallon, E. M.; Haugh, J. M. Scratching the (cell) surface: cytokine engineering for improved ligand/receptor trafficking dynamics. *Chem. Biol.* **1998**, *5*, R257−R263.

(2) Trilletlenoir, V. et al. Recombinant granulocyte colony-stimulating factor reduces the infectious complications of cytotoxic chemotherapy. *Eur. J. Cancer* **1993**, *29A*, 319−324.

(3) Nicola, N. A. *Guidebook to Cytokines and their Receptors*; Oxford University Press: New York, 1994.

(4) Fukunaga, R.; Ishizaka-Ikeda, E.; Nagata, S. Growth and differentiation signals mediated by different regions in the cytoplasmic domain of granulocyte colony-stimulating factor receptor. *Cell* **1993**, *74*, 1079−1087.

(5) Layton, J. E.; Hockman, H.; Sheridan, W. P.; Morstyn, G. Evidence for a novel in vivo control mechanism of granulopoiesis: mature cell-related control of a regulatory growth factor. *Blood* **1989**, *74*, 1303−1307.

(6) Morstyn, G., Dexter, T. M., Foote, M., Eds.; *Filgrastim (r-metHuG-CSF) in Clinical Practice*; Marcel Dekker: New York, 1998.

(7) Delgado, C.; Francis, G. E.; Fisher, D. The uses and properties of PEG-linked proteins. *Crit. Rev. Ther. Drug* **1992**, *9*, 249−304.

(8) Katre, N. V. The conjugation of proteins with polyethylene glycol and other polymers: altering properties of proteins to enhance their therapeutic potential. *Adv. Drug Delivery Rev.* **1993**, *10*, 91−114.

(9) Molineux, G. et al. A new form of Filgrastim with sustained duration in vivo and enhanced ability to mobilize PBPC in both mice and humans. *Exp. Hematol.* **1999**, *27*, 1724−1734.

(10) Johnston, E. et al. Randomized, dose-escalation study of SD/01 compared with daily Filgrastim in patients receiving chemotherapy. *J. Clin. Oncol.* **2000**, *18*, 2522−2528.

(11) Reddy, C. C.; Niyogi, S. K.; Wells, A.; Wiley: H. S.; Lauffenburger, D. A. Engineering epidermal growth factor for enhanced mitogenic potency. *Nat. Biotechnol.* **1996**, *14*, 1696−1699.

(12) French, A. R.; Tadaki, D. K.; Niyogi, S. K.; Lauffenburger, D. A. Intracellular trafficking of epidermal growth factor family ligands is directly influenced by the pH sensitivity of the receptor/ligand interaction. *J. Biol. Chem.* **1995**, *270*, 4334−4340.

(13) Fallon, E. M.; Liparoto, S. F.; Lee, K. J.; Ciardelli, T. L.; Lauffenburger, D. A. Increased endosomal sorting of ligand to recycling enhances potency of an interleukin-2 analog. *J. Biol. Chem.* **2000**, *275*, 6790−6797.

(14) Sarkar, C. A. et al. Rational cytokine design for increased lifetime and enhanced potency using pH-activated 'histidine switching'. *Nat. Biotechnol.* **2002**, *20*, 908−913.

(15) Lu, H. S. et al. Folding and oxidation of recombinant human granulocyte colony stimulating factor produced in *Escherichia coli*. *J. Biol. Chem.* **1992**, *267*, 8770−8777.

(16) Kinstler, O. B. et al. Characterization and stability of N-terminally PEGylated rhG-CSF. *Pharm. Res.* **1996**, *13*, 996−1002.

(17) Horan, T. et al. Dimerization of the extracellular domain of granulocyte-colony stimulating factor receptor by ligand binding: a monovalent ligand induces 2:2 complexes. *Biochemistry* **1996**, *35*, 4886−4896.

(18) Layton, J. E. et al. Interaction of granulocyte colony-stimulating factor (G-CSF) with its receptor: evidence that Glu^{19} of G-CSF interacts with Arg^{288} of the receptor. *J. Biol. Chem.* **1999**, *274*, 17445−17451.

(19) Reidhaar-Olson, J. F.; De Souza-Hart, J. A.; Selick, H. E. Identification of residues critical to the activity of human granulocyte colony-stimulating factor. *Biochemistry* **1996**, *35*, 9034−9041.

(20) Pearce, K. H.; Cunningham, B. C.; Fuh, G.; Teeri, T.; Wells, J. A. Growth hormone binding affinity for its receptor surpasses the requirements for cellular activity. *Biochemistry* **1999**, *38*, 81−89.

(21) Black, J. W.; Leff, P. Operational models of pharmacological agonism. *Proc. R. Soc. London, Ser. B* **1983**, *220*, 141−162.

Accepted for publication January 14, 2003.

BP020017G